



Waves plus currents crossing at a right angle: Experimental investigation

R. E. Musumeci,¹ L. Cavallaro,¹ E. Foti,¹ P. Scandura,¹ and P. Blondeaux²

Received 24 February 2005; revised 13 February 2006; accepted 11 April 2006; published 22 July 2006.

[1] The hydrodynamics generated by a regular wave field perpendicularly superimposed to a steady current is investigated by means of laboratory experiments. The flow structure is analyzed by measuring the velocity profiles using a micro Acoustic Doppler Velocimeter. Three cases are considered: current only, waves only and waves plus current. Different bottom roughnesses are used, and the apparent roughness k_s is estimated for each condition. In the presence of a small roughness, the superposition of the waves on the current causes an increase of the current velocities close to the bottom, thus generating a decrease of the apparent roughness with respect to the case of the current only. On the other hand, when a large bottom roughness is present, the waves force a decrease of the current velocity close to the bottom and, in turn, an increase of the apparent bottom roughness. Such a behavior seems related not only to the roughness but also to the flow regime (i.e., laminar or turbulent) within the wave bottom boundary layer.

Citation: Musumeci, R. E., L. Cavallaro, E. Foti, P. Scandura, and P. Blondeaux (2006), Waves plus currents crossing at a right angle: Experimental investigation, *J. Geophys. Res.*, *111*, C07019, doi:10.1029/2005JC002933.

1. Introduction

[2] The hydrodynamics of the coastal region is usually characterized by the simultaneous presence of waves and currents. The studies available in the literature [see, for example, *Simons et al.*, 1992; *Fredsøe et al.*, 1999] show that a wave field superimposed on a steady current can significantly change the mean velocity profile and the turbulent properties of the current close to the bottom. Since the hydrodynamics at the bottom of a sea wave plays a fundamental role on sediment transport, diffusion of pollutants and other important coastal phenomena, in the last decades a large number of studies have been devoted to investigate wave-current bottom boundary layers [*Soulsby et al.*, 1993].

[3] The complexity of the problem does not allow theoretical investigations to be easily carried out, and therefore the phenomenon has been mainly studied experimentally, even though theoretical analyses do exist [e.g., *Huang and Mei*, 2003].

[4] In the field, such a kind of experimental research is difficult because the continuously changing characteristics of waves and currents, which can cross at any angle, make it impossible to perform a systematic investigation. Moreover, in the field the bottom roughness is difficult to be measured and it can be extremely variable. Indeed, wave-current interaction occurs over smooth beds, such as clay beds or freshly deposited muddy beds, or over rough beds, such as

sand-covered plane beds, rippled beds, or beds covered with stone/armour blocks [*Sumer*, 2003].

[5] Because of the aforementioned difficulties, most experimental studies have been carried out in laboratory, notwithstanding the presence of unavoidable scale effects. In order to overcome the limits (and/or the complications imposed by) of wave basins (namely, small Reynolds numbers and asymmetric waves), oscillating water tunnels have been adopted by several authors [see, among others, *Dedow*, 1966; *Kamphuis*, 1975; *Murray et al.*, 1993].

[6] In the case of waves propagating with the current, the experimental investigations carried out by *Kemp and Simons* [1982] show that the mean velocities near a smooth bed are increased by the presence of waves, whereas near a rough bed they are reduced; the latter finding being confirmed also for waves propagating against the current [*Kemp and Simons*, 1983]. Experiments carried out to study the hydrodynamics generated by waves propagating orthogonally with respect to the current direction show some interesting findings as well. *Visser* [1986] found that over a rough bottom, the mean velocities generated by wave-current interaction are larger than those measured for current only.

[7] In order to simulate an oscillatory motion orthogonal to a current, [*Sleath*, 1990] used an oscillating plate in a flume and found that, over a smooth bed, the oscillations of the plate have an insignificant effect on the current velocity profiles. *Simons et al.* [1992, 1994, 1996] carried out a series of experiments to study the wave-current interaction over a rough bed; they found that the wave presence induces a significant reduction of the mean velocity in the upper part of the flow coupled, in most cases, with an increase close to the bottom. This effect is more pronounced for waves with long periods and large heights. However, as far as the wave-induced velocities and shear stress are concerned, *Simons*

¹Department of Civil and Environmental Engineering, University of Catania, Catania, Italy.

²Department of Environmental Engineering, University of Genova, Genova, Italy.

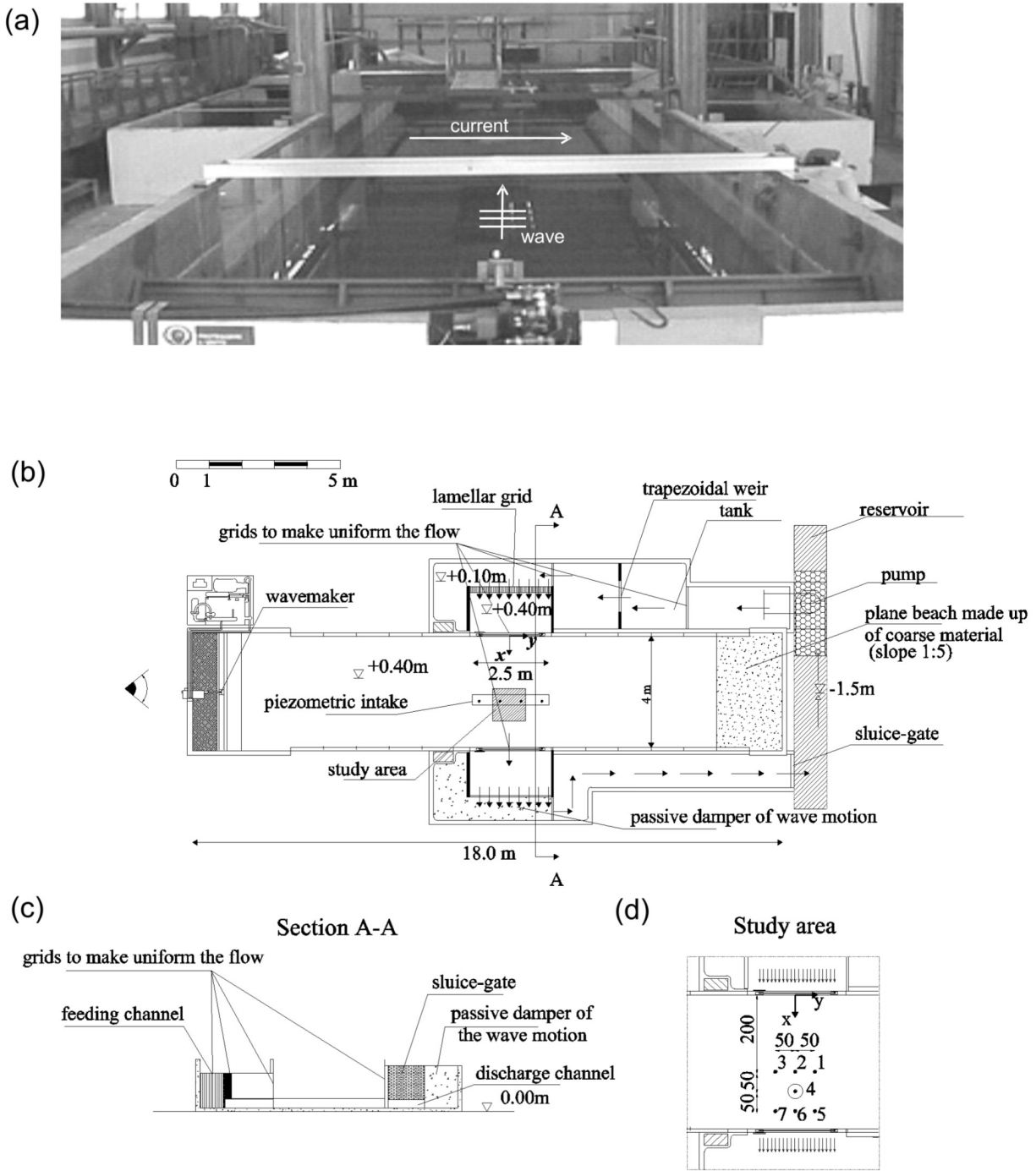


Figure 1. Experimental setup. (a) Bird's-eye view of the wavetank and of the recirculating apparatus from behind the wavemaker, (b) plan view, (c) cross section of the experimental apparatus, and (d) reference system and study area.

and coworkers found that no significant changes occur because of the superimposition of the current. Finally, *Arnskov et al.* [1993] analyzed the instantaneous bed shear stress magnitude and direction over a smooth bed in a combined wave-current motion, with waves propagating both perpendicularly and at an oblique angle and found that the maximum bed shear stress is almost unaffected by the presence of waves.

[8] Even though the aforementioned works contributed significantly to the understanding of wave-current interaction, there are still aspects of the phenomenon which need to be analyzed under well controlled conditions, such as situations in which free surface effects are taken into account, too.

[9] In the present paper the results of an experimental investigation in a wave flume are presented. The work is aimed at understanding how the vertical velocity profile of a

Table 1. Estimated Uncertainties of the Performed Measurements

Quantity	Symbol	Instrument	Uncertainty
Volume flux	Q	trapezoidal weir	$\delta Q_{\max} = 0.0016 \text{ m}^3/\text{s}$
Water depth	h_0	dipstick	$\delta h = 0.002 \text{ m}$
Water depth	h_0	piezometer	$\delta h = 0.0005 \text{ m}$
Position of the control volume	x	rule	$\delta x = 0.005 \text{ m}$
Position of the control volume	y	rule	$\delta y = 0.005 \text{ m}$
Position of the control volume	z	micro-ADV	$\delta z = 0.001 \text{ m}$
Velocity	(v_x, v_y)	micro-ADV	$\delta v_x = \delta v_y = 0.0039 \text{ m/s}$
Velocity	v_z	micro-ADV	$\delta v_z = 0.0031 \text{ m/s}$
Wave period	T	wavemaker	$\delta T_{\max} = 0.0001 \text{ s}$
Wave height	H	wave gauges	$\delta H = 0.001 \text{ m}$

steady current is affected by the presence of a wave which propagates in the direction orthogonal to the current. Since the velocity profile is strictly related to the apparent bottom roughness k_s , which is a key parameter to be used in most of the hydrodynamic and morphodynamic models of the coastal environment, particular attention is paid to better the estimate of such a parameter, in the presence of both waves and currents over either a natural sandy bottom or a gravel bed.

[10] The paper is organized as follows. The next section is devoted to a description of the apparatus and of the experimental procedure, along with a description of the preliminary tests carried out to verify the accuracy and reliability of the experimental measurements. Then, the experimental measurements are presented and the main results concerning the velocity profiles are described, in section 3. In section 4, the experimental data are analyzed to provide estimates of the apparent roughness k_s . Some conclusions are then drawn in the final section.

2. Experimental Setup and Procedure

[11] The experiments have been carried out at the Hydraulics Laboratory of the Department of Civil and Environmental Engineering of the University of Catania. Figure 1 shows the experimental setup, which comprises two interacting systems: (1) a flume for the wave generation and propagation and (2) a recirculating apparatus, which allows for a uniform current interacting with the waves at a right angle to be generated.

[12] The wave flume is 18.00 m long, 4 m wide and 1.20 m high with a fixed horizontal bottom. The waves are generated by means of a flap-type wavemaker, which is driven by a pneumatic system and is electronically controlled.

[13] The apparatus for the generation of the current consists of an underground reservoir, a submerged electro-pump, a series of channels, which feed the current entering the wave tank through the inlet, and a discharge channel beyond the outlet of the tank (see Figure 1). The submerged pump is designed to work with low heads and large discharges. The nominal power of the pump is 11.0 kW, while the maximum discharge is about $0.25 \text{ m}^3/\text{s}$. The pump is continuously monitored during the experiments to check that the volume flux remains constant. The water from the reservoir flows through a series of channels, which stabilize the highly turbulent flow coming out from the pump. A trapezoidal weir is used to measure the volume flux. Finally, before entering the wave tank, a system of uniformly and equally spaced vertical lamellar grids adjusts the direction of the current and makes the velocity profiles as uniform

possible. The grid spacing is 1 cm and the lamellae are 20 cm long in the current direction. Then, the current enters the wave tank through a 2.5 m wide inlet with a direction orthogonal to that of wave propagation. In particular, the entrance is shaped so as to eliminate spurious components of the velocity. The outlet is symmetric with respect to the inlet. Moreover, mattresses of polystyrene fixed at the channel walls absorb spurious wave reflections. The discharge returns back into the pump reservoir through a sluice gate.

[14] The surface elevation is measured by means of several resistance wave gauges. Moreover, in order to measure the mean water level along the middle section of the current, a set of piezometers are also installed (see Figure 1b). A Sontek Micro Acoustic Doppler Velocimeter (a 10 MHz ADV probe plus the ADVLab processor) is used to measure the three velocity components.

[15] The micro-ADV is located on a movable carriage. The sampling volume is a cylinder 9 mm high with a volume equal to 0.3 cm^3 , located 5 cm far from the transmitter. The adopted sampling frequency is 30 Hz.

[16] The measurement uncertainties are presented in Table 1.

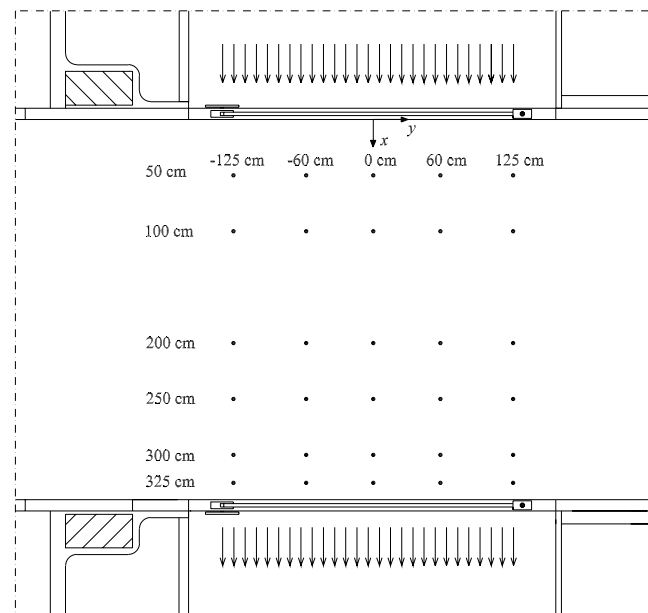


Figure 2. Locations of the measuring stations for the spatial analysis of the wave-current interaction (Matrix experiment). The x direction indicates the current direction.

Table 2. Values of the Control Parameters, Hydrodynamic Characteristics and Dimensionless Parameters for the Spatial Analysis (Matrix Experiment)

Test	h_0 , m	Q , m ³ /s	H , m	T , s	d_{50} , mm	U_c , m/s	U_0 , m/s	U_c/U_0	Re_c	Re_w
M1	0.30	0.037	-	-	0.24	0.049	-	-	14833	-
M2	0.30	0.037	0.086	1.0	0.24	0.049	0.147	0.337	14833	3422

[17] During the experiments, the water temperature measured in the tank is approximately constant, in the range 19°–21°C, therefore the value of the kinematic viscosity is assumed constant and equal to its value at 20°C, i.e., $\nu = 1.00 \cdot 10^{-6}$ m²/s.

[18] The experimental procedure is as follows: (1) The volume flux to be recirculated is fixed, (2) the recirculation pump is run until the water levels in all the channels are stable and a uniform current is established within the wave tank, (3) the velocity profiles of the current are measured within the study area, (4) with the pump still running, the wavemaker is switched on and the wave motion is generated within the tank, (5) when the wave motion reaches a regime condition, the wave characteristics are measured within the study area, (6) velocity profiles are measured in the study area, and (7) the previous three steps are repeated for different wave conditions.

[19] Before presenting the experimental results, it should be pointed out that because of the limits of the ADV, no measurement within the thin wave bottom boundary layer ($O(\sim 1$ mm)) is gathered. Moreover, the obtained velocity profiles refer to the lower part of the water column, since no measurement can be taken between the wave crest and the level 5 cm below the wave trough.

[20] In the following, the reference system is chosen in such a way that the x axis is along the direction of the current propagation, the y axis is along the direction of wave propagation and the z axis is vertical and pointing upward ($z = 0$ lies on the bottom).

3. Data Acquisition and Experimental Results

[21] To obtain a comprehensive understanding of the spatial distribution of the flow generated by the interaction of the current with the propagating waves a first set of experiments is carried out by measuring the velocity profiles over the entire area within which waves and current interact.

[22] Then, to determine the effects of the bottom roughness on the vertical velocity profile when waves and current interact, the flow is analyzed in the presence of different bottom roughnesses. In particular, the flow generated by current only, by waves only and by waves plus current is studied, in the presence of both a small and a large roughness at a particular measuring station.

3.1. Spatial and Temporal Distribution of the Flow

[23] The spatial distribution of the flow within the wave tank has been preliminarily investigated by means of a flow

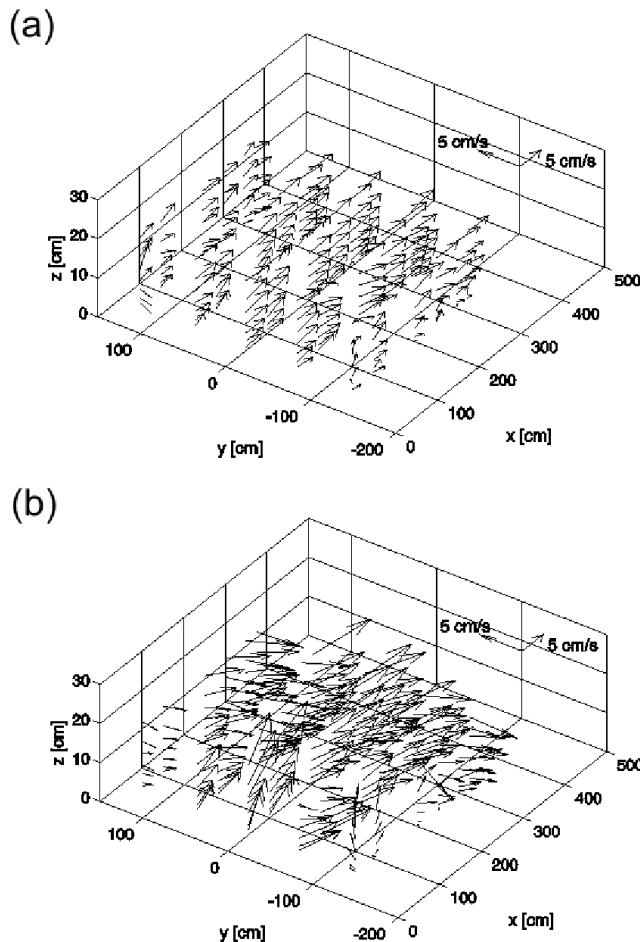


Figure 3. Three-dimensional representation of the time-averaged velocity profiles: (a) current only and (b) waves plus current.

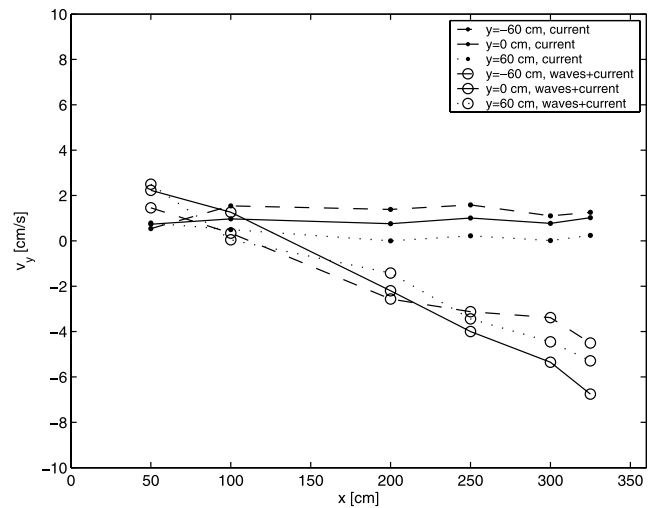


Figure 4. Depth-integrated time-averaged velocity in the wave direction along the current direction. Dots indicate only current, and circles indicate waves plus current. Dashed line indicates $y = -60$ cm, solid line indicates $y = 0$ cm, and dotted line indicates $y = 60$ cm.

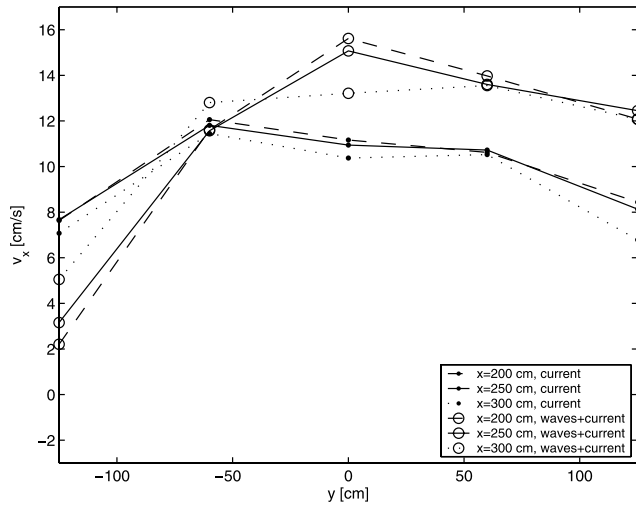


Figure 5. Depth-integrated time-averaged velocity in the current direction along the wave direction. Dots indicate only current, and circles indicate waves plus current. Dashed line indicates $x = 200$ cm, solid line indicates $x = 250$ cm, and dotted line indicates $x = 300$ cm.

visualization technique (milk is used as tracer, because of its specific weight which is very similar to that of water). In particular it has been verified that side effects at the edges of the current inlet are negligible. Then, to make a detailed quantitative spatial analysis, a matrix of 5×6 measuring stations is considered. The location of the stations is shown in Figure 2 (hereinafter this data set is referred to as the “Matrix experiment”). In particular, five longitudinal sections are considered: one at the half-width of the current ($y = 0$ cm); two at intermediate locations ($y = 60$ cm and $y = -60$ cm) and two at the sides of the current ($y = 125$ cm and $y = -125$ cm). Along each section six velocity profiles are gathered. The location of the measuring stations has been chosen so that: two stations are quite close to the inlet area ($x = 50$ cm and $x = 100$ cm), three stations are within the study area ($x = 200$ cm, $x = 250$ cm and $x = 300$ cm) and one station is located very close to the outlet ($x = 325$ cm).

[24] The values of the control parameters, i.e., the water depth h_0 , the volume flux Q , the wave height H and the wave period T , are given in Table 2. Moreover, in order to simulate a roughness similar to that of a sandy bottom, the horizontal fixed bottom is made rough by coating with unimodal well-sorted quartz sand ($d_{50} = 0.24$ mm). In particular, a thin layer of silicone glue was spread uniformly over the bed and then an uniform layer of sediment was sprinkled on top of it.

[25] The hydrodynamic characteristics (mean current velocity U_c and amplitude of the wave velocity oscillations close to the bottom U_0) and the dimensionless parameters (the ratio between U_c/U_0 , the current Reynolds number $Re_c = U_c h_0/\nu$ and the wave Reynolds number $Re_w = U_0^2/\nu\omega$, where $\omega = 2\pi/T$ is the angular frequency of the waves) of the Matrix experiments are also given in Table 2.

[26] The experimental data are averaged over both the time and the phase. The time average is computed by considering a time series about 60 wave cycle long, while phase-averaged quantities are computed by considering 30

Table 3. Depth-Integrated Time-Averaged Velocity Components in the Current and in the Wave Directions, (v_x, v_y) , Expressed in cm/s at All the Measuring Stations of the Matrix Experiment^a

y , cm	x , cm					
	50	100	200	250	300	325
125	(5.02, 0.00), (2.28, -1.48)	(7.24, 0.80), (6.09, -0.55)	(8.44, 0.69), (12.08, -0.53)	(8.13, 0.89), (12.45, -2.31)	(6.79, 0.66), (12.07, -3.25)	(7.61, 0.24), (9.76, -4.32)
60	(9.15, 0.54), (12.37, 1.46)	(9.97, 1.54), (12.90, 0.34)	(10.62, 1.39), (13.98, -2.57)	(10.72, 1.58), (13.60, -3.12)	(10.53, 1.10), (13.55, -3.38)	(11.23, 1.26), (13.23, -4.50)
0	(10.64, 0.73), (13.44, 2.23)	(10.99, 0.97), (15.81, 1.26)	(11.16, 0.76), (15.62, -2.20)	(10.94, 1.01), (15.07, -4.00)	(10.37, 0.77), (13.21, -5.35)	(10.4, 1.02), (12.67, -6.76)
-60	(10.52, 0.78), (15.50, 2.50)	(10.83, 0.50), (14.24, 0.05)	(12.06, 0.00), (11.61, -1.42)	(11.81, 0.22), (11.57, -3.44)	(11.45, 0.01), (12.80, -4.45)	(11.35, 0.24), (13.17, -5.29)
-125	(3.45, 0.72), (-0.86, 0.21)	(7.02, 0.71), (0.48, -0.80)	(7.63, 0.25), (2.21, -2.38)	(7.67, 0.29), (3.16, -3.50)	(7.08, 0.10), (5.05, -4.89)	(6.41, 0.19), (4.79, -5.83)

^aFirst set of values, current only; second set of values, waves plus currents.

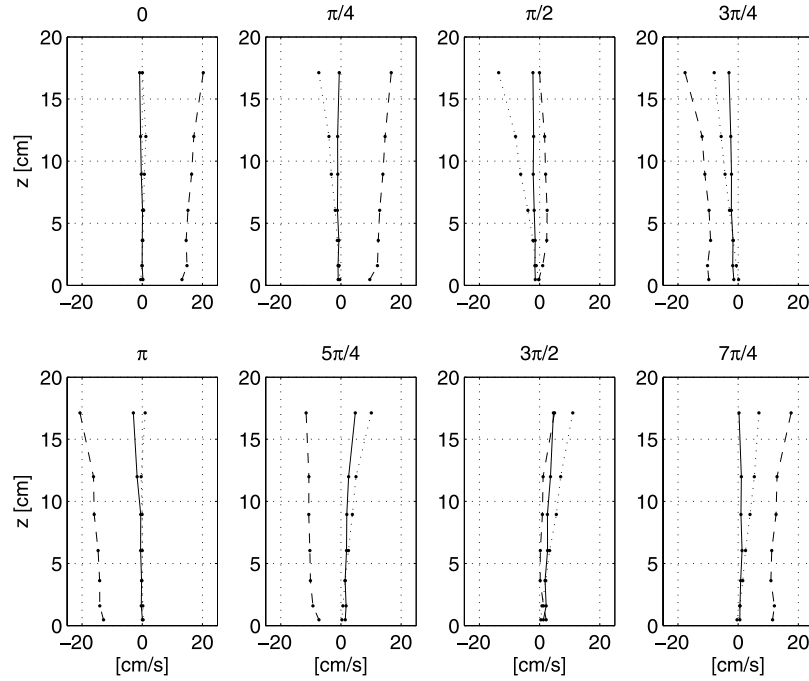


Figure 6. Oscillating part of the phase-averaged velocity profiles at the phases 0 , $\pi/4$, $\pi/2$, $3\pi/4$, π , $5\pi/4$, $3\pi/2$, and $7\pi/4$ (phase equal to 0 corresponds to the wave crest) at $x = 250$ cm, $y = 0$ cm ($Q = 0.037$ m³/s, $H = 0.086$ m, $T = 1.0$ s, $h = 0.30$ m, $d_{50} = 0.24$ mm). Solid line indicates v_x , dashed line indicates v_y , and dotted line indicates v_z .

Table 4. Values of the Control Parameters, Hydrodynamic Parameters and Dimensionless Parameters for the Analysis of the Bottom Roughness Influence^a

Test	Q , m ³ /s	H , m	T , s	d_{50} , mm	U_c , m/s	U_0 , m/s	U_c/U_0	Re_c	Re_w
R1	0.033	-	-	0.24	0.044	-	-	13,252	-
R2	-	0.085	0.8	0.24	-	0.095	-	-	1,155
R3	-	0.086	1.0	0.24	-	0.147	-	-	3,438
R4	-	0.085	1.2	0.24	-	0.175	-	-	5,822
R5	-	0.089	1.4	0.24	-	0.201	-	-	8,987
R6	-	0.102	0.8	0.24	-	0.115	-	-	1,676
R7	-	0.101	1.0	0.24	-	0.172	-	-	4,717
R8	-	0.101	1.2	0.24	-	0.206	-	-	8,117
R9	-	0.102	1.4	0.24	-	0.231	-	-	11,861
R10	0.033	0.083	0.8	0.24	0.044	0.093	0.475	13,252	1,101
R11	0.033	0.088	1.0	0.24	0.044	0.149	0.296	13,252	3,551
R12	0.033	0.085	1.2	0.24	0.044	0.174	0.255	13,252	5,754
R13	0.033	0.085	1.4	0.24	0.044	0.193	0.229	13,252	8,311
R14	0.033	0.102	0.8	0.24	0.044	0.114	0.386	13,252	1,666
R15	0.033	0.106	1.0	0.24	0.044	0.181	0.244	13,252	5,214
R16	0.033	0.103	1.2	0.24	0.044	0.210	0.210	13,252	8,443
R17	0.033	0.104	1.4	0.24	0.044	0.235	0.235	13,252	12,260
R18	0.035	-	-	30.00	0.047	-	-	14,192	-
R19	-	0.083	0.8	30.00	-	0.094	-	-	1,123
R20	-	0.084	1.0	30.00	-	0.143	-	-	3,273
R21	-	0.083	1.2	30.00	-	0.170	-	-	5,512
R22	-	0.085	1.4	30.00	-	0.192	-	-	8,195
R23	-	0.109	0.8	30.00	-	0.122	-	-	1,907
R24	-	0.108	1.0	30.00	-	0.184	-	-	5,392
R25	-	0.105	1.2	30.00	-	0.214	-	-	8,758
R26	-	0.103	1.4	30.00	-	0.233	-	-	12,048
R27	0.035	0.085	0.8	30.00	0.047	0.096	0.493	14,192	1,172
R28	0.035	0.086	1.0	30.00	0.047	0.146	0.324	14,192	3,398
R29	0.035	0.086	1.2	30.00	0.047	0.176	0.269	14,192	5,918
R30	0.035	0.086	1.4	30.00	0.047	0.194	0.244	14,192	8,409
R31	0.035	0.102	0.8	30.00	0.047	0.115	0.411	14,192	1,689
R32	0.035	0.103	1.0	30.00	0.047	0.176	0.269	14,192	4,905
R33	0.035	0.106	1.2	30.00	0.047	0.218	0.217	14,192	9,045
R34	0.035	0.101	1.4	30.00	0.047	0.229	0.207	14,192	11,676

^aThe water depth h_0 is kept equal to 0.30 m for all the experiments. Tests $R1 \div R17$ are for small roughness, and tests $R18 \div R34$ are for large roughness.

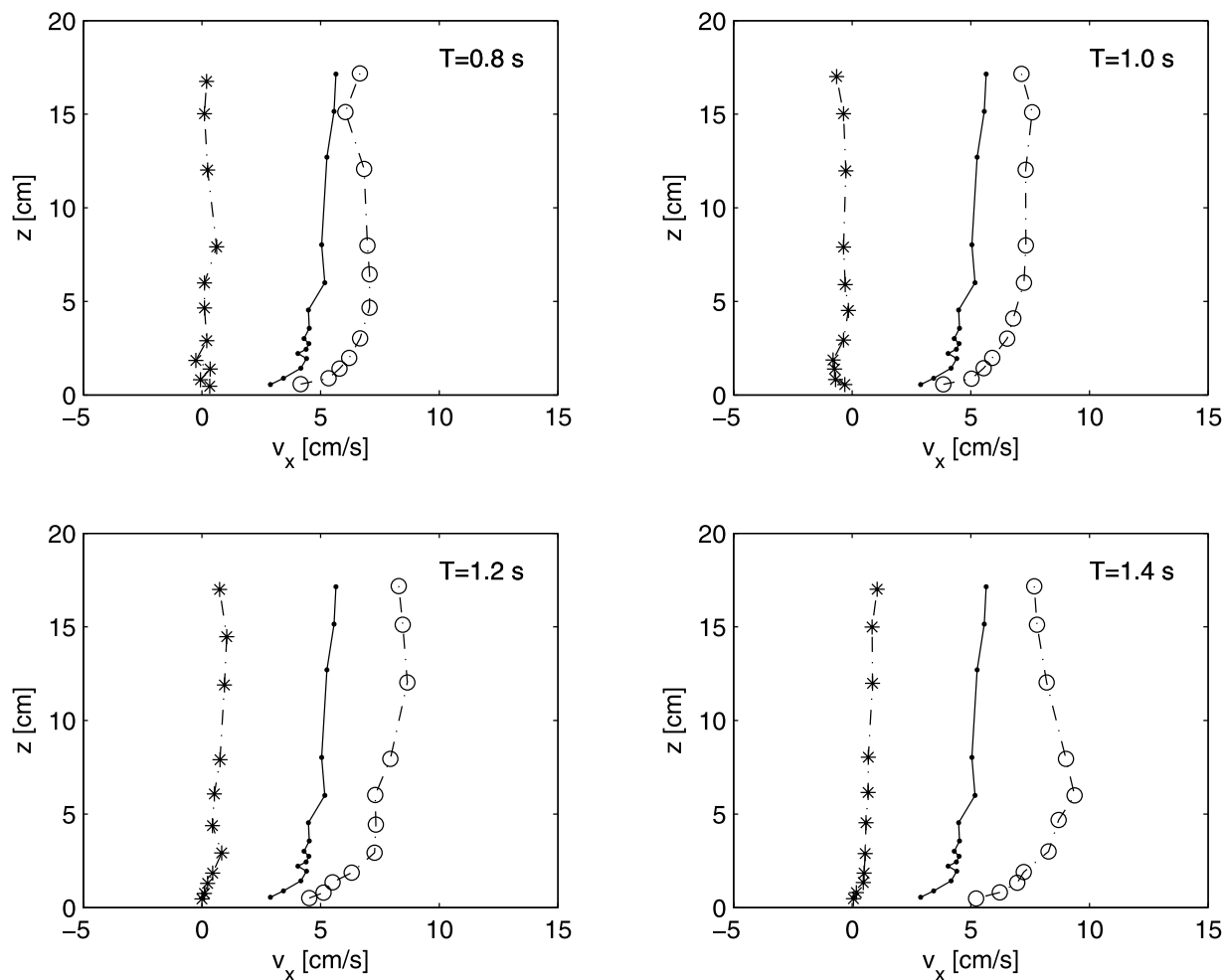


Figure 7. Time-averaged velocity profiles in the current direction for the small roughness case. Dots indicate current only, stars indicate waves only, and circles indicate waves plus current ($Q = 0.033 \text{ m}^3/\text{s}$, $H = 8.5 \text{ cm}$, $h_0 = 30 \text{ cm}$, $d_{50} = 0.24 \text{ mm}$).

wave cycles. By computing the averaged quantities using a larger number of wave cycles, it has been verified that the time series are long enough to provide reliable results.

[27] The time-averaged velocity profiles, measured in the study area, show that, when the current only is present, the flow is quite homogeneous in the range $-60 \text{ cm} \leq y \leq 60 \text{ cm}$ (see Figure 3a). Small disturbances are observed at the two edges of the jet, where a shear layer is generated because of the interaction between the current and the still fluid in the tank, and the mean flow velocities decrease, as expected.

[28] In Figure 3b, the 3-D representation of the time-averaged velocity profiles, as obtained from measurements taken when the orthogonal wave motion is superimposed on the current, shows that the flow patterns become more complex, as the mean flow bends in the direction opposite to that of wave propagation (particularly for $x > 100 \text{ cm}$). Such a behavior is due to the undertow current, which arises in the lower part of the water column to balance the mass transport due to wave propagation.

[29] The phenomenon can be more easily appreciated looking at Figure 4, where the depth and time-averaged value of the y velocity component is plotted versus x for the

current only and the waves plus current cases for $y = -60, 0, \text{ and } 60 \text{ cm}$. Indeed, the presence of the waves causes large negative velocity values which tend to bend the current. Figure 5, where the depth and time-averaged value of the x velocity component is plotted versus y for the current only and the waves plus current cases for $x = 200, 250, \text{ and } 300 \text{ cm}$, shows clearly for the current only case the typical gaussian bell shape of the jet flowing from the inlet toward the outlet in still waters, whereas the presence of the waves causes the bending of the jet, i.e., the asymmetry of the bell shape itself, thus the velocities are larger for positive values of y than for negative value of y . In Table 3 the depth and time-averaged values of the two velocity components are given for all the measuring stations. As already pointed out the reader should notice that the average along the vertical direction has been made along the lower part of the water column, since no measurements close to the free surface have been made.

[30] In order to investigate the structure of the wave-current flow during one wave cycle, a phase average of the velocity profiles in the current direction is performed too.

[31] The oscillating part of the three velocity components (v_x, v_y, v_z) during the wave cycle at $x = 250 \text{ cm}$ and $y = 0 \text{ m}$ is

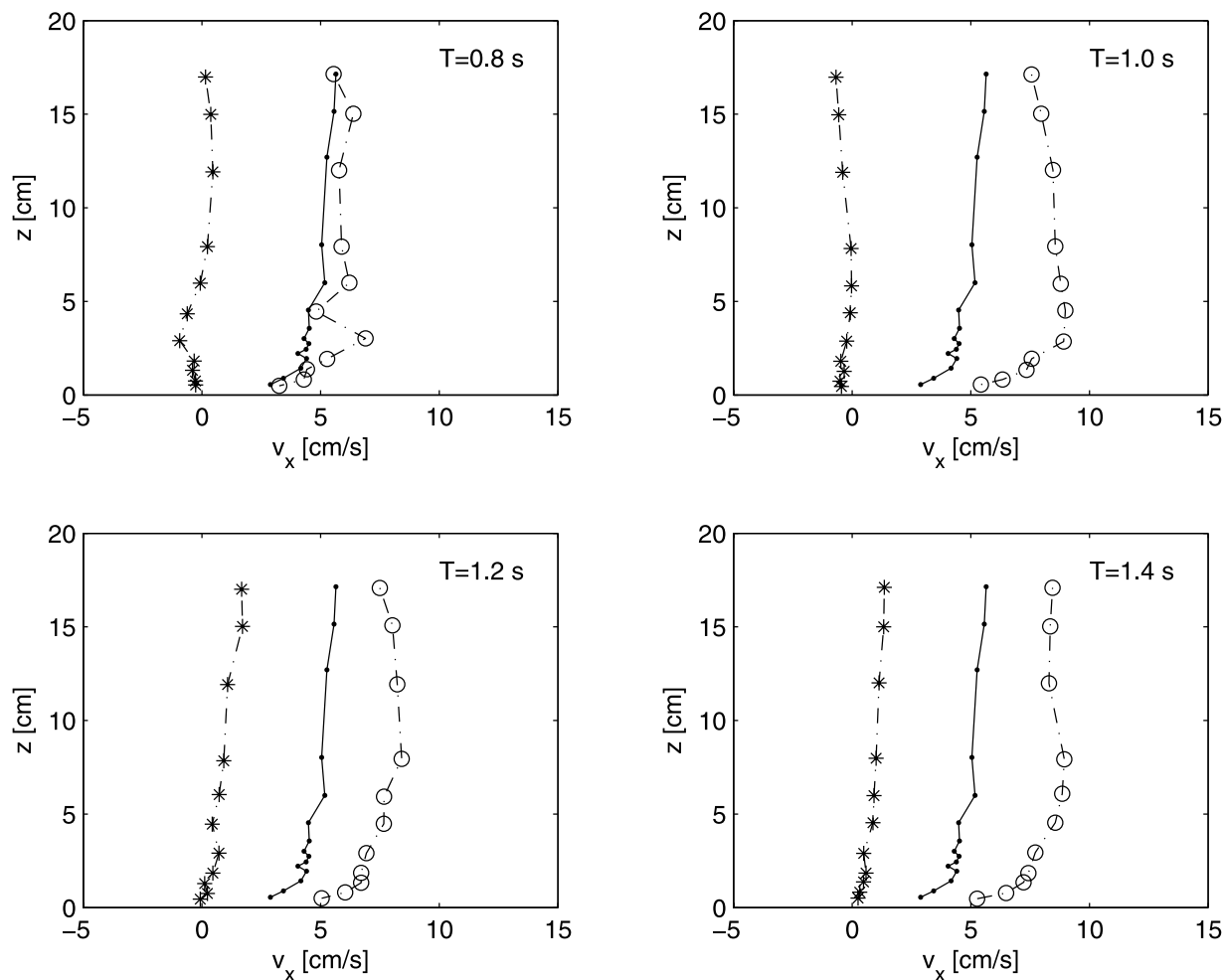


Figure 8. Time-averaged velocity profiles in the current direction for the small roughness case. Dots indicate current only, stars indicate waves only, and circles indicate waves plus current ($Q = 0.033 \text{ m}^3/\text{s}$, $H = 10.0 \text{ cm}$, $h_0 = 30 \text{ cm}$, $d_{50} = 0.24 \text{ mm}$).

shown in Figure 6. It should be pointed out that the phase equal to 0 corresponds to the wave crest (zero-down crossing of the vertical velocity component) and that the oscillating component of the velocity is calculated by subtracting the time-averaged value from the phase-averaged velocity.

[32] By comparing the profiles it can be seen that the vertical velocity v_z is always $\pi/2$ out of phase with respect to the velocity component v_y along the direction of wave propagation, as predicted by the linear wave theory. However, it is interesting to notice that there is also a small oscillating velocity component v_x which is also out of phase with respect to v_y .

3.2. Influence of the Bottom Roughness

[33] The influence of the bottom roughness is investigated by using two different values and looking at the results in one measuring station only, namely station 4 ($x = 250 \text{ cm}$, $y = 0 \text{ cm}$). It is worth pointing out that such a point can be considered representative of the flow within the fully interaction region. In particular, a small roughness is obtained by gluing onto the bottom well-sorted sand with

a $d_{50} = 0.24 \text{ mm}$, while a large roughness is obtained by coating the bed with gravels characterized by a mean diameter of about 30 mm.

[34] In Table 4, the values of the control parameters, namely the volume flux Q , the wave height H , the wave period T and the mean size of the bottom sediments d_{50} are reported along with other hydrodynamic quantities and dimensionless parameters (mean current velocity U_c , amplitude of the wave velocity oscillation close to the bottom U_0 , ratio U_c/U_0 , current Reynolds number Re_c and wave Reynolds number Re_w). The water depth h_0 is kept fixed and equal to 0.30 m in all the tests. No waves with a period longer than 1.4 s, i.e., no wavelength longer than 2 m, are generated. Since the width of the steady current in the y direction is about 2.5 m, at least one whole wave is present within the region where the current interacts with the waves.

3.2.1. Small Roughness Case

[35] The vertical profiles of the time-averaged velocity component v_x in the current direction are plotted in Figures 7 and 8, for the small roughness ($d_{50} = 0.24 \text{ mm}$), in three cases of current, waves and waves plus current. The wave

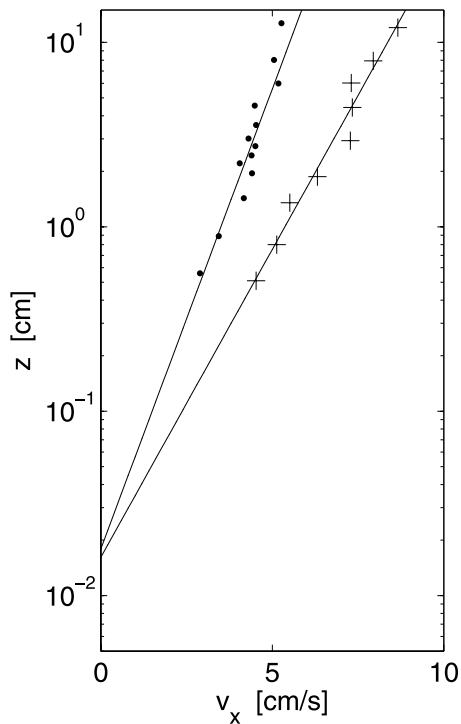


Figure 9. Time-averaged velocity profiles in a semilogarithmic plane. Dots indicate current only, pluses indicate waves plus current, and solid lines indicate interpolating straight line ($Q = 0.033 \text{ m}^3/\text{s}$, $H = 8.5 \text{ cm}$, $T = 1.2 \text{ s}$, $h_0 = 30 \text{ cm}$, $d_{50} = 0.24 \text{ mm}$).

period ranges between 0.8 s and 1.4 s and the wave height is 8.5 cm and 10.0 cm, in Figure 7 and in Figure 8, respectively. The current velocity profile without waves is plotted in each panel as a reference profile. When only the wave motion is present, as expected, the mean velocities are negligible in the direction orthogonal to wave propagation. Such velocities do not completely vanish because a x component of the velocity is generated when the waves interact with the inlet and the outlet of the recirculating apparatus. Close to the bed, the velocity profiles (averaged over a wave cycle) for the current case and the wave plus current case follow the logarithmic law. Such a behavior is clearly shown in Figure 9, where two sets of data are reported in a semilogarithmic plane along with interpolating straight lines. The interaction of the waves with the current leads to an increase of the current velocity which is larger close to the bottom. Furthermore, the increase becomes larger as the wave period is increased. Finally, by comparing Figures 7 and 8, it appears that such an increase is also affected by the change of the wave height.

[36] The aforementioned results seem to violate mass conservation. Therefore the recirculating volume flux has been carefully checked during all the experiments and it has been verified that it keeps constant. Hence the increase of the velocity in the lower part of the water column, where the measurements are carried out, should be balanced by an equivalent decrease of the velocity in the upper part of the water column. This fact is experimentally confirmed by some qualitative measurements obtained using of a micro-propeller and by some quantitative measurements gathered

for particular experimental conditions (very small wave heights) for which the use of the micro-ADV in the upper part of the water column is possible. Moreover, it is worth pointing out that similar results were obtained also by *Simons et al.* [1992].

[37] In Figures 10 and 11, the mean velocity profiles in the wave direction, obtained with current only, waves only and waves plus current, are plotted for two different wave heights ($H = 8.5 \text{ cm}$ and $H = 10 \text{ cm}$, respectively). In the wave direction, the mean current velocities are zero when the waves are absent, whereas both in the wave case and in the wave-current case the velocity in the y direction is not zero because of the undertow current which is significant. The observed values agree fairly well with those predicted by the linear wave theory. However, the presence of the current leads to an increase of the steady streaming close to the bottom and to a decrease of the velocity gradient along the vertical direction. This is particularly evident if the wave period and/or the wave height increases. Thus the effect of the current is to homogenize the mean velocity profile. Such an effect is probably due to the strong turbulence associated with the current.

3.2.2. Large Roughness Case

[38] Figures 12 and 13 show the vertical velocity profiles of the time-averaged velocity component v_x in the current direction for the large roughness case ($d_{50} = 30 \text{ mm}$). Two wave heights are considered, namely $H = 8.5 \text{ cm}$ and $H = 10.0 \text{ cm}$, and the wave period T ranges between 0.8 s and 1.4 s.

[39] In the presence of the very rough bed, both in the current case and in the waves plus current case, the mean velocity profiles follow the logarithmic law as over the small roughness bed. However, the general results over the rough bed differ significantly from those observed in the presence of the small roughness. Indeed, the waves plus current velocity in the x direction is smaller than the velocity measured when the waves are absent. Such a velocity decrease is due to the large resistance induced at the bottom by the turbulent eddies generated by the macro-roughness, interacting with the oscillating velocity induced by the waves. The velocity decrease is smaller for increasing wave period T , even though the dependency on T seems quite weak when compared with the small roughness case. The distance from the bed where the current and the waves plus current velocity profiles have the same value (intersection point) decreases when the wave height is increased; that is, the vertical velocity gradient $\frac{\partial v_x}{\partial z}$ becomes larger as the wave height increases.

[40] The velocity profiles in the wave direction are shown in Figures 14 and 15, for $H = 8.5 \text{ cm}$ and $H = 10.0 \text{ cm}$, respectively. A small increase of v_y is still observed when the current is added to the wave field. Moreover, the effect of adding the current to the waves is to homogenize the velocity profile as in the small roughness case. However, the current affects the wave motion less than it does in the presence of a small roughness.

4. Analysis of Results and Discussion

4.1. Phase Shift in the Current Direction

[41] The current is driven by a gradient of the water level $\frac{\partial d}{\partial x}$, where d is the total water depth, $d = h_0 + \eta$ (h_0 is the

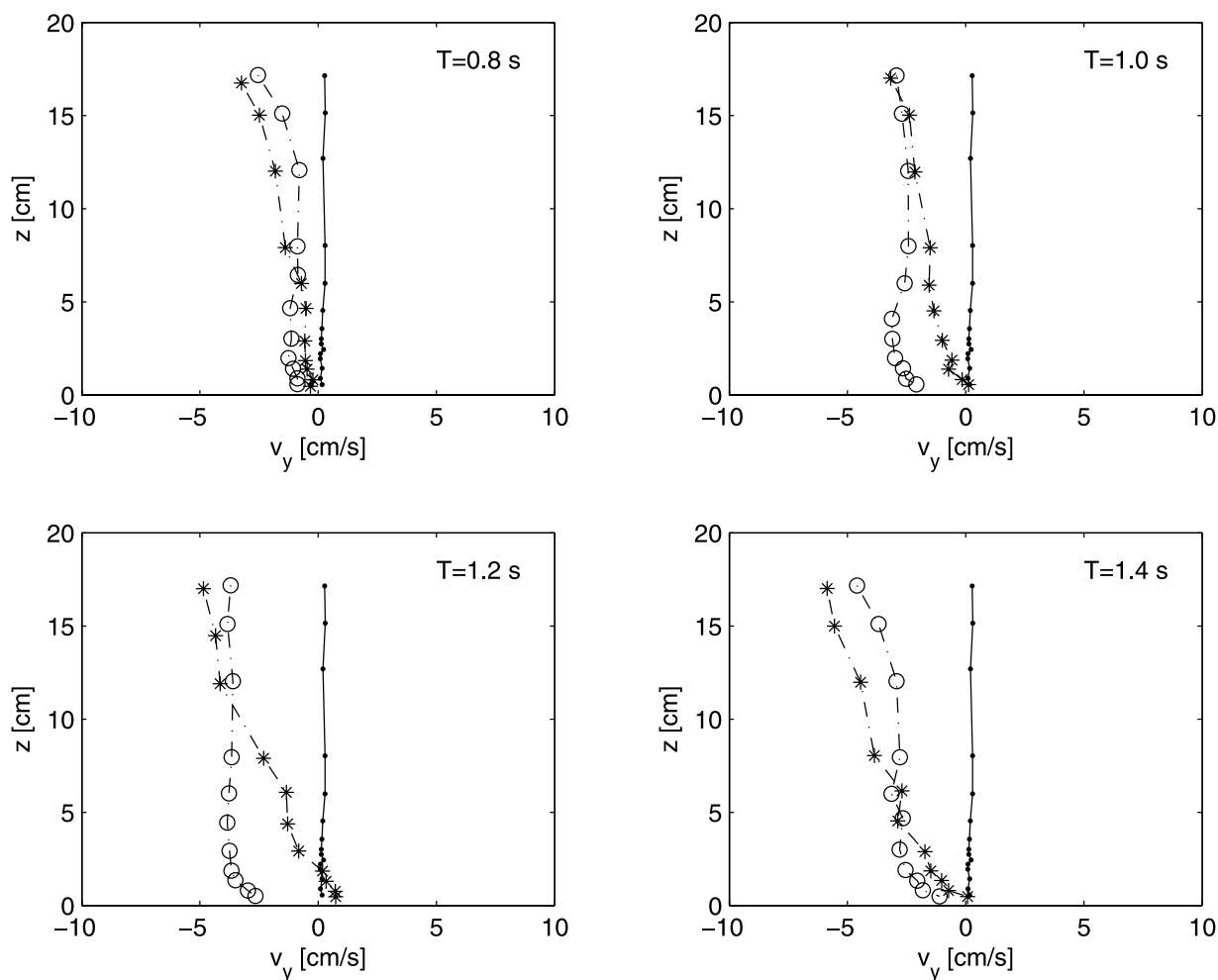


Figure 10. Time-averaged velocity profiles in the wave direction for the small roughness case. Dots indicate current only, stars indicate waves only, and circles indicate waves plus current ($Q = 0.033 \text{ m}^3/\text{s}$, $H = 8.5 \text{ cm}$, $h_0 = 30 \text{ cm}$, $d_{50} = 0.24 \text{ mm}$).

mean water depth and η is the instantaneous surface elevation).

[42] When the wave motion is added to the steady current, the oscillating part of the surface elevation η affects the structure of the flow in the current direction. Indeed the time-dependent surface displacement forces a gradient of the water level which drives a periodic flow. As a consequence, the motion in the current direction has both a steady component and an oscillatory one, as it is shown in Figure 16. Moreover, such a forcing acts differently along the current, generating a phase lag between the x and the y velocity components which changes in the x direction. For instance, at the inlet section, the water level gradient $\frac{\partial d}{\partial x}$ is maximum and the instantaneous current velocity v_x is minimum, at the wave crests. Moreover, the water level gradient $\frac{\partial d}{\partial x}$ is minimum and the current velocity v_x is maximum at the wave troughs. On the other hand, at the outlet, v_x is maximum when wave crests are present and is minimum at the wave troughs. Since the wave front is orthogonal to the current direction, the wave crest reaches at the same time

both the inlet and the outlet, forcing a decrease of the current velocity at one end and an increase at the other one. Therefore a space-varying phase lag between the velocity components should be present.

[43] A simple model of the phenomenon previously described can be formulated assuming waves of small amplitudes generating an oscillatory velocity component of the same order of magnitude as the steady current [see *Musumeci et al.*, 2004]. The model shows that evanescent oscillating modes are generated by the interaction of the wave motion with the inlet and the outlet boundaries. Such modes are characterized by an amplitude which decays away from the inlet and the outlet and vanishes after a length of the order of magnitude of a few water depths. Since in the present experimental apparatus the current length is about 4 m and the water depth is $h_0 = 0.30 \text{ m}$, it is expected that the evanescent modes give a significant contribution to the flow field.

[44] An estimate of the phase lag, defined as the time interval between the maximum velocity in the x direction and the maximum velocity in the y direction, can be

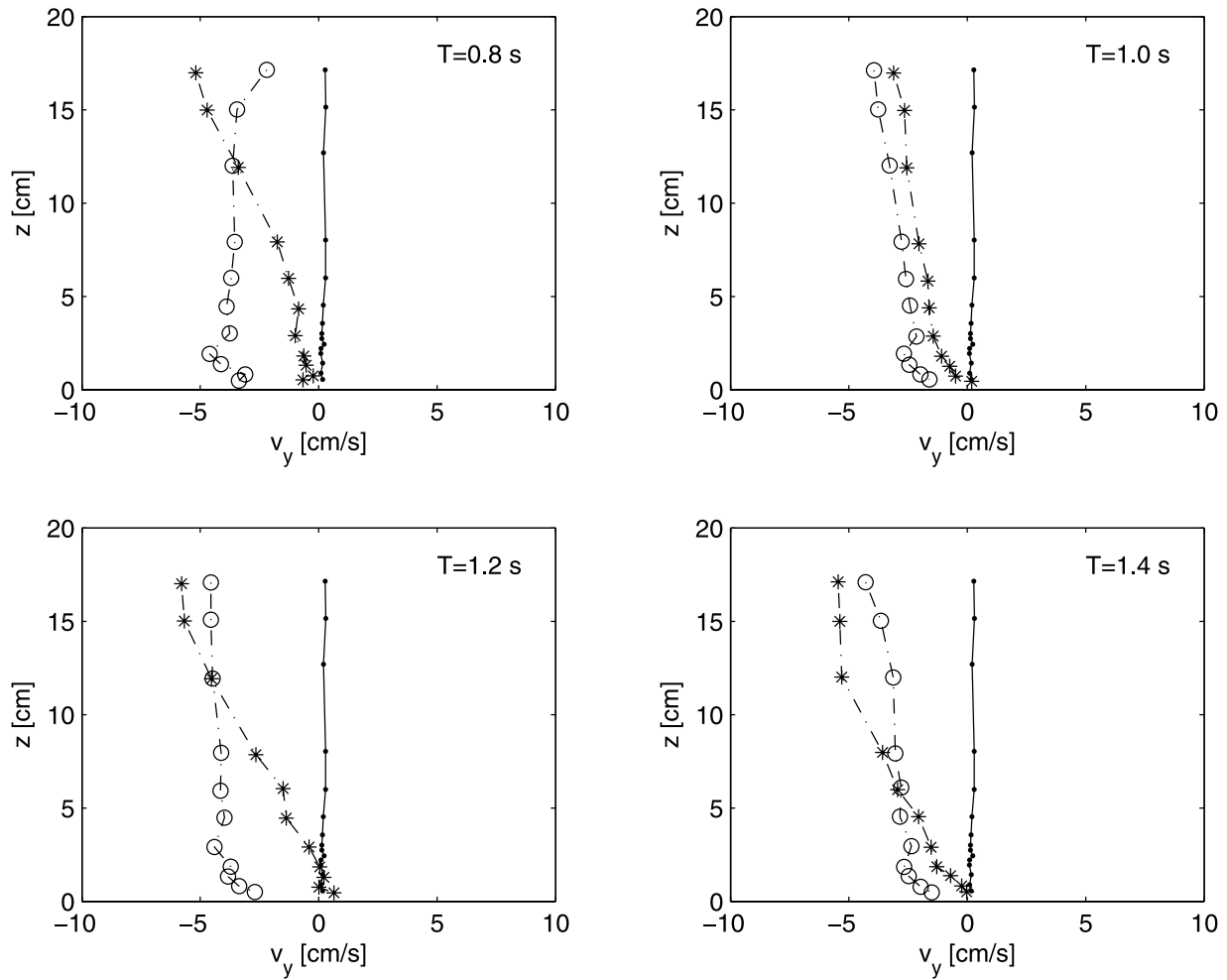


Figure 11. Time-averaged velocity profiles in the wave direction for the small roughness case. Dots indicate current only, stars indicate waves only, and circles indicate waves plus current ($Q = 0.033 \text{ m}^3/\text{s}$, $H = 10.0 \text{ cm}$, $h_0 = 30 \text{ cm}$, $d_{50} = 0.24 \text{ mm}$).

obtained from Figure 16 where the phase-averaged values of the velocity oscillations are plotted along the line $y = 0 \text{ cm}$, which lies in the symmetry plane of the current. The measuring points are close to the inlet ($x = 50$ and 100 cm), inside the study area ($x = 200, 250,$ and 300 cm) and close to the outlet ($x = 325 \text{ cm}$).

[45] Figure 16 shows that a phase lag exists between v_x and v_y , which varies in the current direction. Attention is focused on the time variation of the velocity signals at the elevation $z \simeq 15 \text{ cm}$, which corresponds to a position in the middle of the water column; that is, the highest where measurements could be made by means of the micro-ADV.

4.2. Apparent Roughness Estimate

[46] As previously pointed out, the flow is significantly affected by the size of the bottom roughness. In particular, the results gathered in the presence of the small and the large bottom roughnesses are quite different. Such differences can be discussed in terms of the apparent roughness k_s , which is a parameter of fundamental interest for coastal hydrodynamics/morphodynamics.

4.2.1. Theoretical Background

[47] The current velocity profile close to the bottom can be described by the well known logarithmic law

$$\frac{v_x}{v_x^*} = \frac{1}{k} \ln \left(\frac{30z}{k_s} + B \right) \quad (1)$$

where v_x is the mean velocity in the current direction, v_x^* is the friction velocity, k is the von Karman constant, z is the vertical distance from the bottom, k_s is the apparent bottom roughness, B is a function of $k_s^+ = \frac{v_x^* k_s}{\nu}$ that can be derived by interpolating the results of Nikuradse. Here the formula of *Krishnappan and Lau* [1986] has been used

$$B = [2.50 \ln k_s^+ - 3.0] e^{-0.217(\ln k_s^+)^2} \quad \text{if } 0 < k_s^+ \leq 70 \quad (2)$$

When $k_s^+ > 70$ the flow is in the fully turbulent regime and B can be assumed equal to zero. On the basis of Equation 1, it can be noted that an estimate of k_s can be obtained simply from the knowledge of the measured velocity profiles. The logical scheme of the procedure

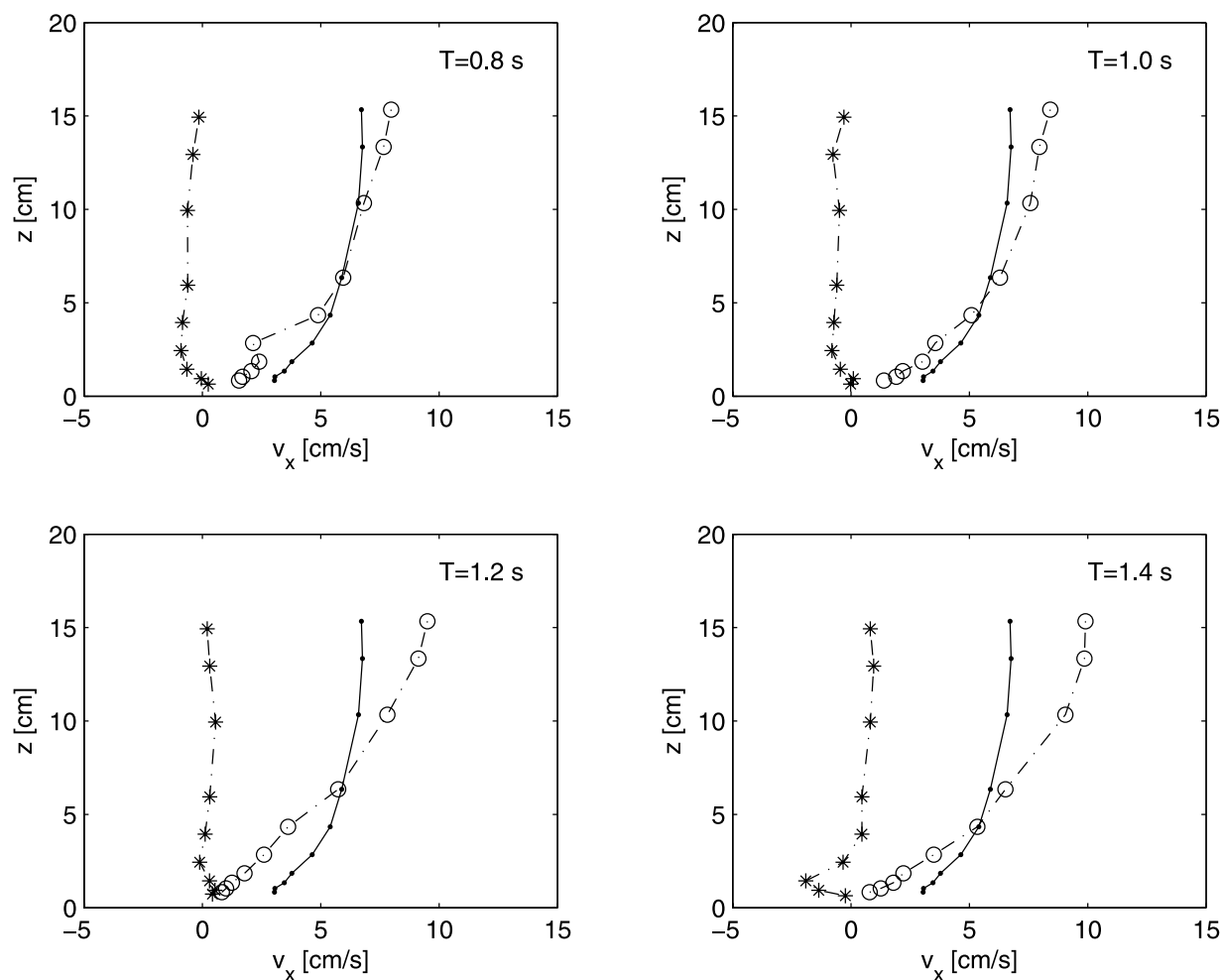


Figure 12. Time-averaged velocity profiles in the current direction for the large roughness case. Dots indicate current only, stars indicate waves only, and circles indicate waves plus current ($Q = 0.035 \text{ m}^3/\text{s}$, $H = 8.5 \text{ cm}$, $h_0 = 30 \text{ cm}$, $d_{50} = 30.0 \text{ mm}$).

adopted to estimate k_s is similar to the one adopted by *Fredsøe et al.* [1999].

[48] A simple least-square method, with $\ln z$ as horizontal axis and v_x as vertical axis, has been adopted in order to determine the values of k_s and v_x^* .

[49] The best fit of the experimental data is influenced by the thickness of the adopted logarithmic layer. According to *Fredsøe et al.* [1999], the upper limit \bar{z} of the logarithmic layer is at $(0.2 \div 0.3)h_0$, with h_0 being the flow depth (such a choice being justified on the basis of *Monin and Yaglom* [1973]), and the lower limit is at $0.2k_s$, to ensure that the variation of the velocity v_x is not influenced by the bottom roughness [*Grass*, 1971].

[50] A sensitivity analysis on the choice of the upper boundary location is carried out, by choosing two thresholds \bar{z} to analyze the results. In particular, in order to fit the data to the logarithmic law, both the small value $0.2h_0$ and the large value $0.3h_0$ are considered, i.e., $\bar{z} = 9 \text{ cm}$ and $\bar{z} = 6 \text{ cm}$. In order to show how the choice of the upper threshold may affect the estimate of k_s and of v_x^* , in Figure 17 the experimental data are plotted along with their linear interpolation, by using the two aforementioned thresholds. Since

the velocity profiles deviate from the logarithmic law as soon as the vertical coordinates becomes larger than $0.2h_0$, it follows that the estimate of k_s may be strongly different in the two cases (up to a factor of 3, over the small roughness bed, much less over the large roughness bed). Therefore, because of the general better fitting of the data, the small limit, i.e., that equal to $0.2h_0$, of the upper boundary of the logarithmic layer is chosen in the following to evaluate the apparent roughness k_s .

[51] With regard to the lower boundary location $0.2k_s$, which depends on the evaluation of the apparent roughness itself, it is verified that such a constraint is fulfilled after k_s is determined.

[52] The apparent bottom roughness in the current direction is estimated both in the current-alone case and in the combined waves plus current case.

4.2.2. k_s Estimate

[53] In Table 5 the values of k_s , both for the small roughness and the large roughness, are given along with the main hydrodynamic parameters of the experiments and the values of the shear velocity v_x^* , of the parameters k_s^+ and a/k_s , where a is the wave-induced orbital excursion

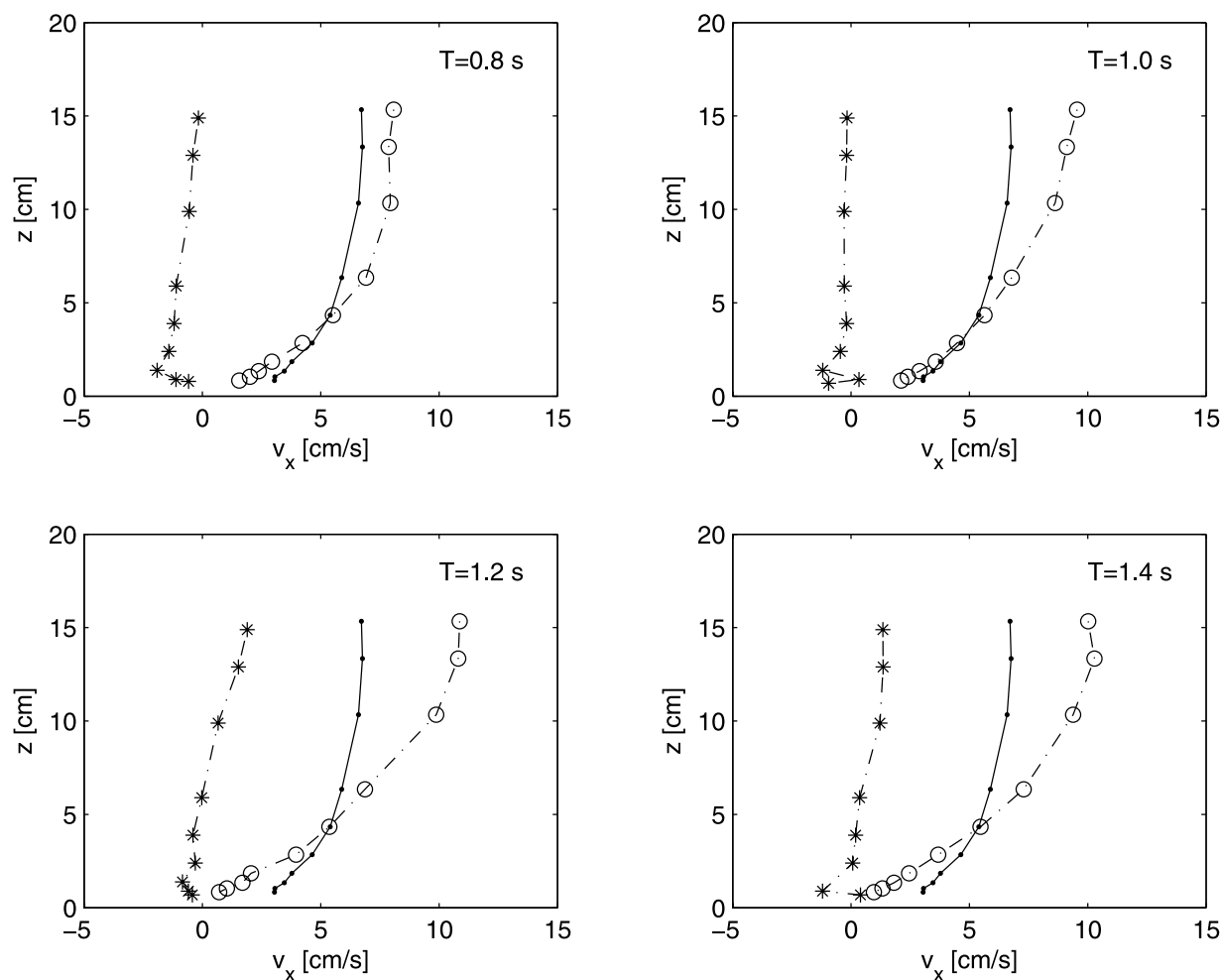


Figure 13. Time-averaged velocity profiles in the current direction for the large roughness case. Dots indicate current only, stars indicate waves only, and circles indicate waves plus current ($Q = 0.035 \text{ m}^3/\text{s}$, $H = 10.0 \text{ cm}$, $h_0 = 30 \text{ cm}$, $d_{50} = 30.0 \text{ mm}$).

sion. From the values of k_s^+ , it can be observed that the large roughness bed experiments were in the hydrodynamically rough regime, whereas those for the small roughness were mostly in the transitional regime and only one experiment (test R16) was in the hydrodynamically smooth regime.

[54] Figures 18 and 19 show the time-averaged velocity profiles, measured over the small and the large roughness respectively, plotted on a semilogarithmic plot along with their best fits. The cases of current only and of waves plus current (for two different values of wave height) are reported.

[55] It can be noticed that the wave boundary layer can be considered laminar when the bottom roughness is small. Indeed, the critical value of the Reynolds number Re_w for a smooth wall (incidentally we point out that $d_{50} = 0.24 \text{ mm}$ is smaller than $\delta = \sqrt{2\nu/\omega}$ in all the experiments) is about $1.5 \cdot 10^5$, which is larger than the Reynolds numbers used in the present experiments (see Table 4). In this case, the velocity increase in the current direction may induce a decrease of the apparent bottom roughness (in the range $0.1 \div 0.9$ of the current only

value). Viceversa, in the presence of the rough bottom, the boundary layer is fully turbulent [Kamphuis, 1975] and the wave motion generates a decrease of the steady velocity component at the bottom. This fact leads to a remarkable increase of k_s (by a factor of $2.6 \div 5.8$) with respect to the current only case.

[56] The apparent roughness decrease due to the wave-current interaction in the small roughness case is quite moderate, while for the large roughness case, the corresponding increase is quite large. Moreover, in the latter case, the results are more stable and their trend is clear, while in the former case in some tests the data show a slight increase of k_s .

[57] The present results seem to contradict the hypothesis usually introduced both in theoretical and numerical models [Grant and Madsen, 1979; Davies et al., 1988], where the wave-generated turbulence is assumed to represent always an extra resistance for the current motion or, in other words, the apparent roughness is assumed always to increase when waves are superimposed to a steady current. From the data obtained during the present experimental investigation, it can be argued that such an assumption is verified only if the

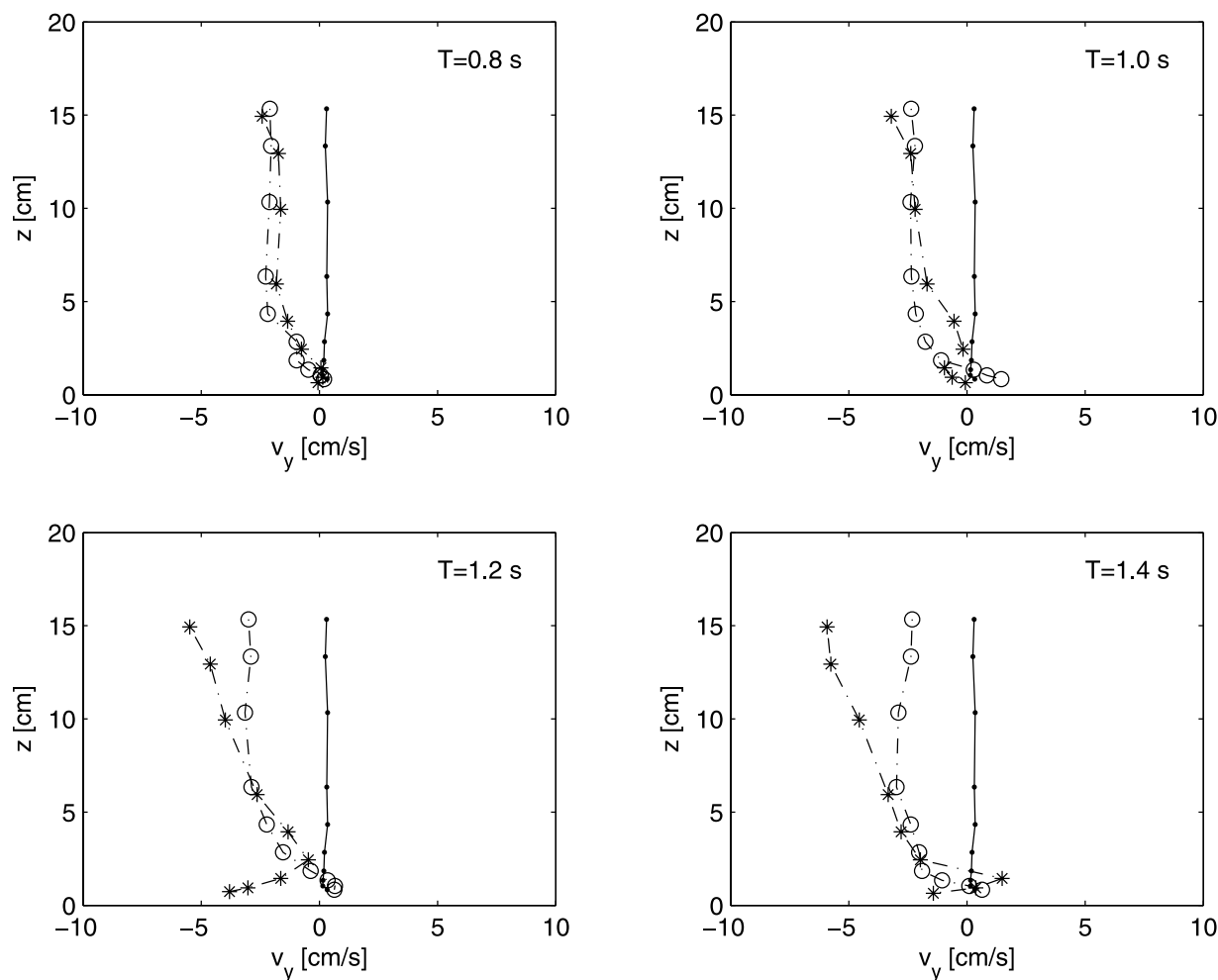


Figure 14. Time-averaged velocity profiles in the wave direction for the large roughness case. Dots indicate current only, stars indicate waves only, and circles indicate waves plus current ($Q = 0.035 \text{ m}^3/\text{s}$, $H = 8.5 \text{ cm}$, $h_0 = 30 \text{ cm}$, $d_{50} = 30.0 \text{ mm}$).

bottom can be considered hydraulically rough, otherwise the apparent roughness may exhibit a decrease. Experimentally, such findings are consistent with those of *Kemp and Simons* [1982] and *Kemp and Simons* [1983] who found similar trends for waves propagating with and against the current.

[58] Also *Lodahl et al.* [1998], in the case of a combined oscillatory plus steady flow within a pipe, found that the mean wall shear stress can be smaller or larger than its current only value. They suggested that the different behavior depends on the flow regime (wave dominated $U_c/U_0 < 1$ versus current dominated $U_c/U_0 > 1$) and on the wave boundary layer structure (laminar versus turbulent). In particular it seems that the wall shear stress may increase only if the flow is wave dominated and the wave bottom boundary layer is fully turbulent, whereas, if the flow is wave dominated but the wave bottom boundary layer is in the laminar regime, a relaminarization of the turbulent current occurs, which leads to a decrease of the wall shear stress. The results of the present study seem to confirm such

an assumption also for the case of waves plus an orthogonal current.

5. Conclusions

[59] The flow generated by waves and a current interacting at a right angle is experimentally investigated in a wave flume.

[60] The problem of the design of the experimental apparatus for the current generation was carefully addressed, thus reducing edge and side effects. The measuring stations are located within an area 1 m^2 wide, where the characteristics of the current and of the waves can be considered uniform.

[61] A detailed analysis of the spatial behavior of the flow throughout the whole area where waves and current interact is carried out.

[62] The effects of the bottom roughness on the wave-current hydrodynamics are investigated by means of velocity measurements, which are performed both in the presence of a relatively moderate roughness ($d_{50} = 0.24 \text{ mm}$) and a very rough bed ($d_{50} = 30 \text{ mm}$). Even though the macro-

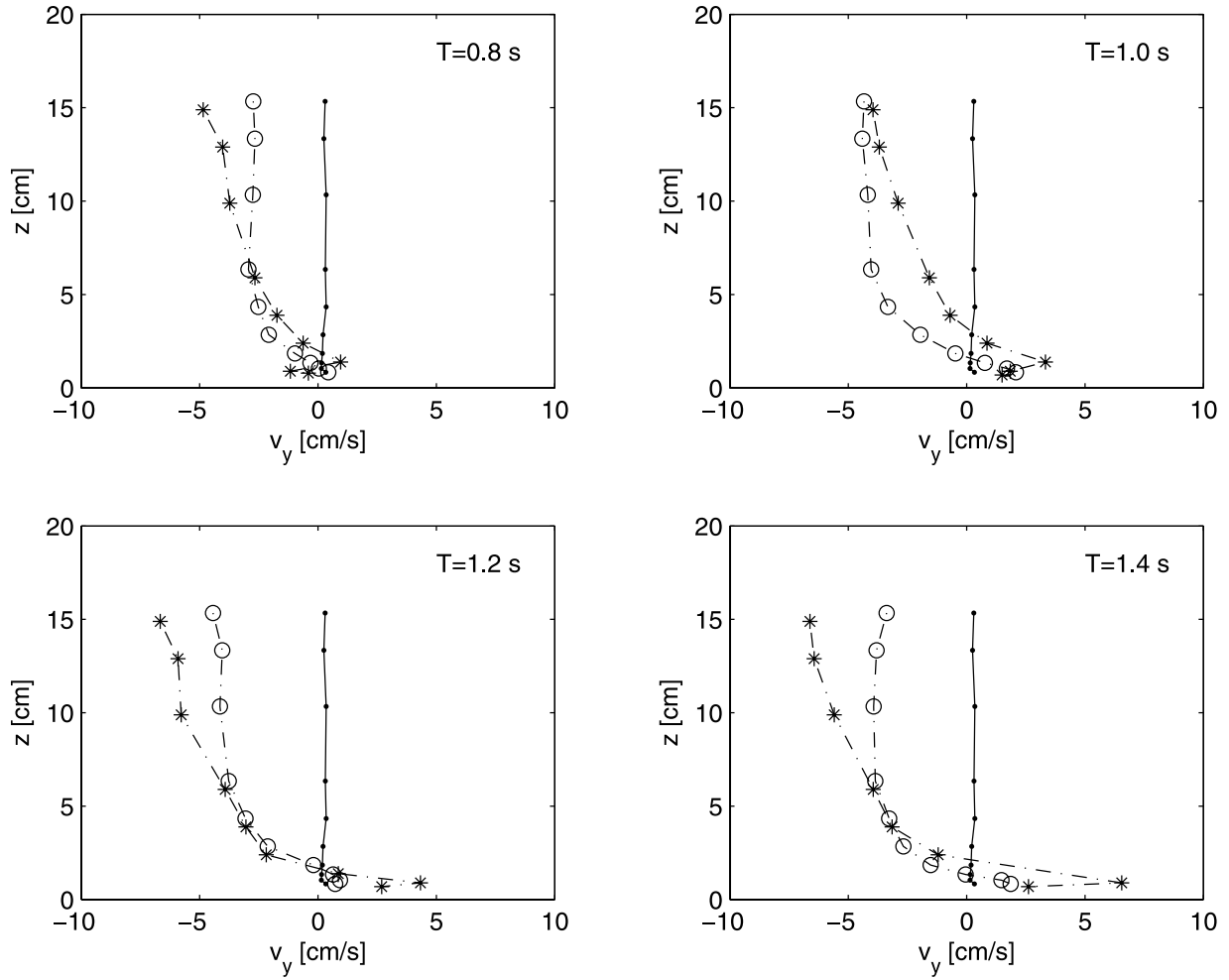


Figure 15. Time-averaged velocity profiles in the wave direction for the large roughness case. Dots indicate current only, stars indicate waves only, and circles indicate waves plus current ($Q = 0.035 \text{ m}^3/\text{s}$, $H = 10.0 \text{ cm}$, $h_0 = 30 \text{ cm}$, $d_{50} = 30.0 \text{ mm}$).

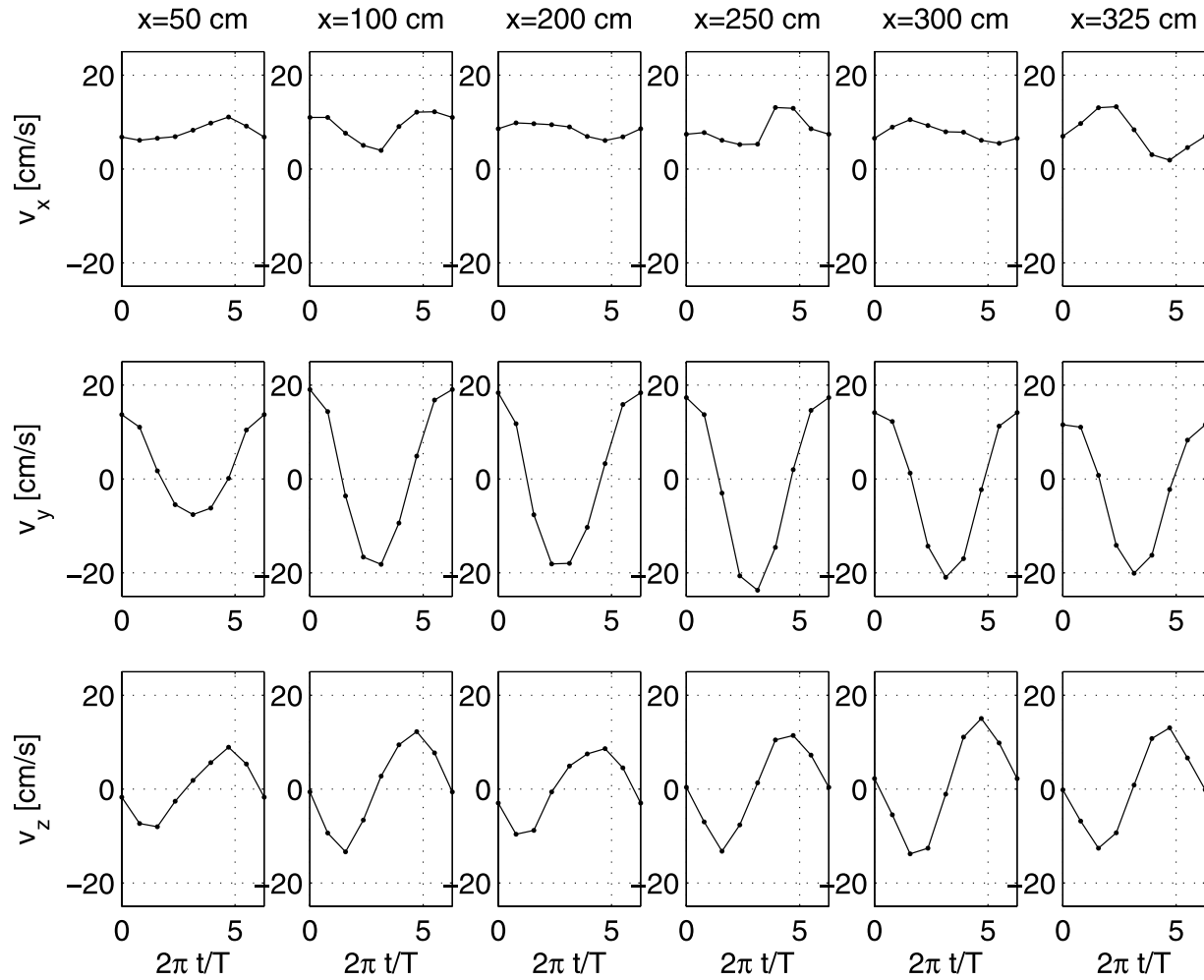


Figure 16. Phase-averaged velocity during a wave cycle ($y = 0$ cm; $z = 15$ cm) at several locations within the wavetank (from left to right: $x = 50, 100, 200, 250, 300,$ and 325 cm) ($Q = 0.037$ m³/s, $H = 0.086$ m, $T = 1.0$ s, $h = 0.30$ m, $d_{50} = 0.24$ mm).

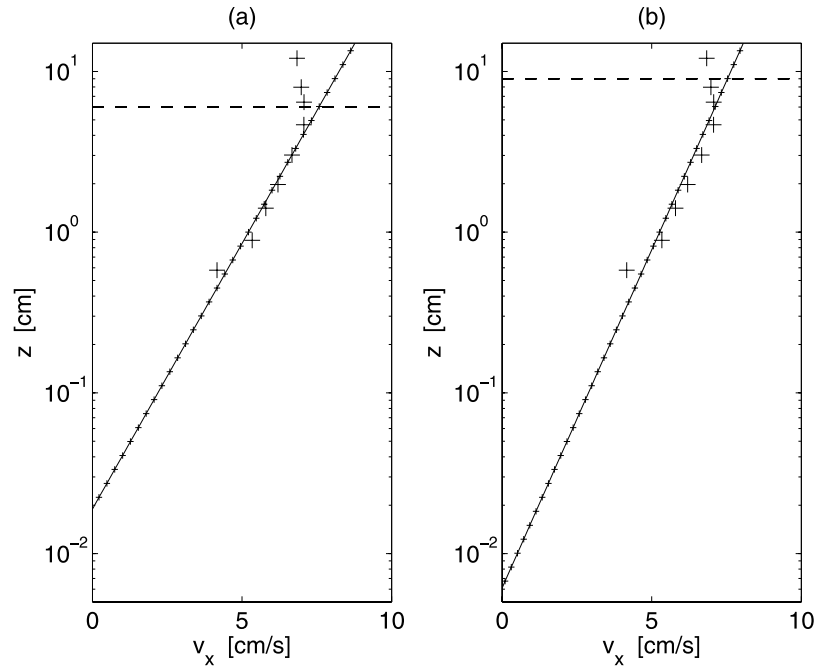


Figure 17. Linear interpolation of the logarithmic velocity profiles using two thresholds: (a) $\bar{z} = 0.2h$ and (b) $\bar{z} = 0.3h$. Pluses indicate experimental data, and pluses with a solid line indicate linear interpolation ($Q = 0.033 \text{ m}^3/\text{s}$, $H = 0.083 \text{ m}$, $T = 1.0 \text{ s}$, $d_{50} = 0.24 \text{ mm}$).

scopic control hydrodynamic parameters (water depth, volume flux, wave period and wave height) are similar, the hydrodynamics generated by the two different roughnesses are different.

[63] Indeed, at least in the range of the parameters of the present work, for the small roughness the wave boundary layer is laminar, while for the large roughness the wave boundary layer becomes turbulent.

Table 5. Estimate of the Apparent Bottom Roughness k_s and of the Shear Velocity v_x^* in the Presence of a Small Roughness ($d_{50} = 0.24 \text{ mm}$) and of a Large Roughness ($d = 30 \text{ mm}$)^a

Test	Q , m^3/s	H , m	T , s	k_s , m	$v_{x_s}^*$, m/s	k_s^+ (-)	$\frac{a}{k_s}$ (-)
<i>Small Roughness</i>							
Current							
R1	0.033	-	-	0.0051	0.003	15	-
Waves plus current							
R10	0.033	0.083	0.8	0.0067	0.005	33	1.79
R11	0.033	0.088	1.0	0.0100	0.006	60	2.40
R12	0.033	0.085	1.2	0.0072	0.006	43	4.58
R13	0.033	0.085	1.4	0.0060	0.006	36	7.17
Waves plus current							
R14	0.033	0.102	0.8	0.0064	0.004	26	2.34
R15	0.033	0.106	1.0	0.0045	0.006	27	6.44
R16	0.033	0.103	1.2	0.0005	0.004	2	80.00
R17	0.033	0.104	1.4	0.0029	0.005	14	17.93
<i>Large Roughness</i>							
Current							
R18	0.035	-	-	0.0378	0.006	226	-
Waves plus current							
R27	0.035	0.085	0.8	0.1177	0.007	781	0.10
R28	0.035	0.086	1.0	0.1345	0.008	1143	0.17
R29	0.035	0.086	1.2	0.1757	0.007	1201	0.19
R30	0.035	0.086	1.4	0.2026	0.011	2143	0.21
Waves plus current							
R31	0.035	0.102	0.8	0.1406	0.010	1341	0.11
R32	0.035	0.103	1.0	0.1005	0.009	863	0.28
R33	0.035	0.106	1.2	0.2189	0.011	2512	0.19
R34	0.035	0.101	1.4	0.1946	0.011	2083	0.26

^aThe depth is $h_0 = 0.3 \text{ m}$ in all the experiments ($\bar{z} = 0.2h$).

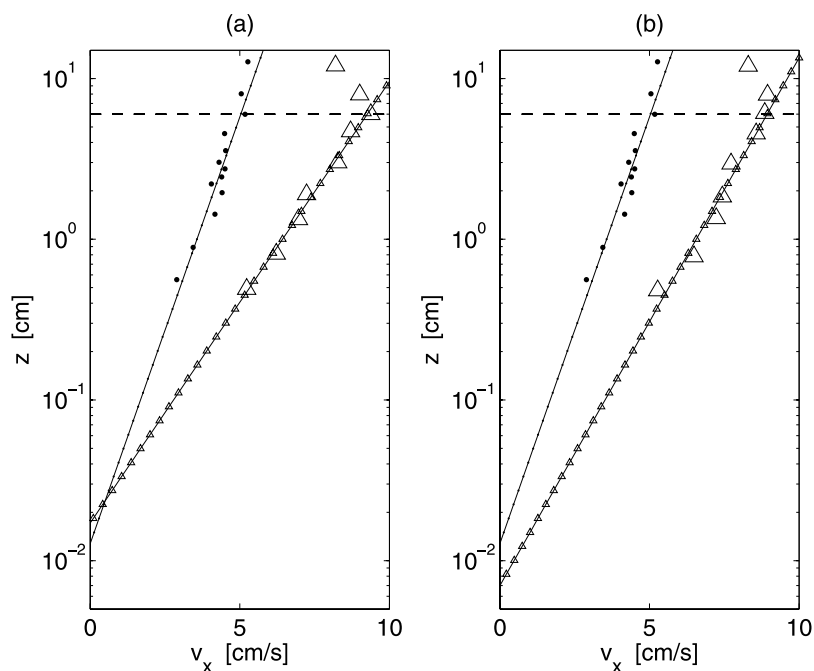


Figure 18. Measured time-averaged velocity profiles over a small roughness bottom ($d_{50} = 0.24$ mm) for current only and wave plus current, and relative linear best fit for the k_s estimate ($\bar{z} = 6$ cm). (a) Threshold depth (dashed line), current only (dots) ($Q = 0.033$ m³/s), and waves plus current (triangles) ($Q = 0.033$ m³/s, $H = 0.085$ m, $T = 1.4$ s). (b) Threshold (dashed line), current only (dots) ($Q = 0.033$ m³/s), and waves plus current (triangles) ($Q = 0.033$ m³/s, $H = 0.104$ m, $T = 1.4$ s).

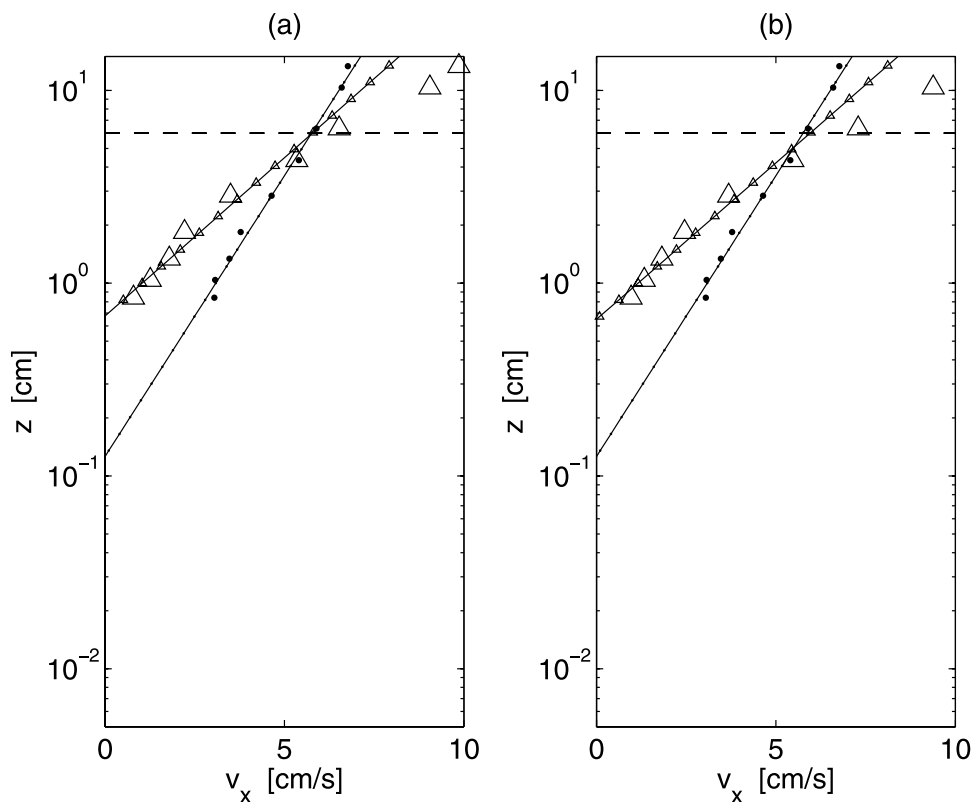


Figure 19. Measured time-averaged velocity profiles over a large roughness bottom ($d_{50} = 30$ mm) for current only and wave plus current and relative linear best fit for the k_s estimate ($\bar{z} = 6$ cm). (a) Threshold depth (dashed line), current only (dots) ($Q = 0.035$ m³/s), and waves plus current (triangles) ($Q = 0.035$ m³/s, $H = 0.086$ m, $T = 1.4$ s). (b) Threshold depth (dashed line), current only (dots) ($Q = 0.035$ m³/s), and waves plus current (triangles) ($Q = 0.035$ m³/s, $H = 0.101$ m, $T = 1.4$ s).

[64] As a result, the velocities in the current direction close to the bottom are larger in the waves plus current case and smaller with respect to the current only case, when the bottom is covered by the small and the large roughness, respectively. Moreover, the effect of the strong turbulence generated by the current on the wave field is to homogenize the velocity profile and to reduce, or even to cancel, the steady streaming within the bottom boundary layer.

[65] The aforementioned processes affect significantly the apparent roughness k_s . In particular, if the roughness is small, the apparent roughness k_s may decrease when the waves are added to the current, whereas if the roughness is large the apparent roughness k_s increases up to one order of magnitude.

[66] Finally, a phase-averaged analysis of the data reveals that the component v_x of the velocity in the current direction has an oscillating part which is out of phase with respect to the wave velocity, v_y . Moreover, such a phase lag between the oscillating part of v_x and v_y does not remain constant along the x axis. Such a phenomenon can be explained by considering that the free surface slope which forces the current has an oscillating part which is due to the presence of the waves. Because of the free surface displacement induced by the waves at the inlet (outlet), the current velocity decreases (increases) where the wave crests are present, whereas the current velocity increases (decreases) when the wave troughs are present.

[67] **Acknowledgments.** Mutlu Sumer of Technical University of Denmark, Ian Ribberink of University of Twente, and Alan Davies and Jonathan Malarkey of University of Wales Bangor are greatly acknowledged for many helpful discussions on several issues arising from the work. Carla Faraci and Ezio Chiara are acknowledged for the help provided in carrying out some of the experiments. The two anonymous referees are also acknowledged for their enlightening comments on the manuscript. This work has been funded by the EC in the framework of the SandPit project (contract EVK3-CT-2001-00056).

References

- Arnskov, M. M., J. Fredsøe, and B. M. Sumer (1993), Bed shear stress measurements over a smooth bed in three-dimensional wave-current motion, *Coastal Eng.*, 20, 277–316.
- Davies, A. G., R. L. Soulsby, and H. L. King (1988), A numerical model of the combined wave and current bottom boundary layer, *J. Geophys. Res.*, 93(C1), 491–508.
- Dedow, H. A. (1966), Friction factor under oscillatory waves, *Houille Blanche*, 7, 837–841.
- Fredsøe, J., K. H. Andersen, and B. M. Sumer (1999), Wave plus current over a ripple-covered bed, *Coastal Eng.*, 38, 177–221.
- Grant, W. D., and O. S. Madsen (1979), Combined wave and current interaction with a rough bottom, *J. Geophys. Res.*, 84(C4), 1797–1808.
- Grass, A. (1971), Structural features of turbulent flow over smooth and rough boundaries, *J. Fluid Mech.*, 50(2), 233–255.
- Huang, Z., and C. Mei (2003), Effects of surface waves on a turbulent current over a smooth or rough seabed, *J. Fluid Mech.*, 497, 253–287.
- Kamphuis, J. W. (1975), Friction factor under oscillatory waves, *J. Waterw. Port Coastal Ocean Eng.*, 101, 135–144.
- Kemp, P. H., and R. R. Simons (1982), The interaction between waves and turbulent current: Waves propagating with current, *J. Fluid Mech.*, 116, 227–250.
- Kemp, P. H., and R. R. Simons (1983), The interaction between waves and turbulent current: Waves propagating against current, *J. Fluid Mech.*, 130, 73–89.
- Krishnapan, B. G., and Y. L. Lau (1986), Turbulence modeling of flood plain flows, *J. Hydraul. Eng.*, 112(4), 251–266.
- Lodahl, C. R., B. M. Sumer, and J. Fredsøe (1998), Turbulent combined oscillatory flow and current in a pipe, *J. Fluid Mech.*, 373, 313–348.
- Monin, A., and A. Yaglom (1973), *Statistical Fluid Mechanics: Mechanics of Turbulence*, MIT Press, Cambridge, Mass.
- Murray, P., R. Soulsby, and A. Davies (1993), Sediment pick-up in combined wave current flow, *Data Rep. SR 364*, HR Wallingford, Wallingford, U. K.
- Musumeci, R. E., L. Cavallaro, E. Foti, P. Scandura, and P. Blondeaux (2004), Modelling wave-current interaction, *Rep. DICA-UNICT-01-04*, Dep. of Civ. and Environ. Eng., Univ. of Catania, Catania, Italy.
- Simons, R. R., T. J. Grass, and M. Mansour-Tehrani (1992), Bottom shear stresses in the boundary layer under waves and currents crossing at right angle, paper presented at 23rd International Conference on Coastal Engineering, Am. Soc. of Civ. Eng., Venice, Italy.
- Simons, R. R., T. J. Grass, W. M. Saleh, and M. Mansour-Tehrani (1994), Bottom shear stresses under random waves with a current superimposed, paper presented at 24th International Conference on Coastal Engineering, Am. Soc. of Civ. Eng., Kobe, Japan.
- Simons, R. R., R. D. MacIver, and W. M. Saleh (1996), Kinematics and shear stresses from combined waves and longshore currents in the UK Coastal Research Facility, paper presented at 25th International Conference on Coastal Engineering, Am. Soc. of Civ. Eng., Orlando, Fla.
- Sleath, J. F. A. (1990), Velocities and bed friction in combined flows, paper presented at 22nd International Conference on Coastal Engineering, Am. Soc. of Civ. Eng., Delft, Netherlands.
- Soulsby, R. L., L. Hamm, G. Klopman, D. Myrhaug, R. Simons, and G. P. Thomas (1993), Wave current interaction within and outside the bottom boundary layer, *Coastal Eng.*, 21, 41–69.
- Sumer, M. B. (2003), Experimental investigation of wave boundary layer, paper presented at Euromech Colloquium: “Sea Wave Bottom Boundary Layer”, Eur. Mech. Soc., Taormina, Italy.
- Visser, P. J. (1986), Wave basin experiments on bottom friction due to current and waves, paper presented at 20th International Conference on Coastal Engineering, Am. Soc. of Civ. Eng., Taipei, Taiwan.

P. Blondeaux, Department of Environmental Engineering, University of Genova, Via Montallegro 1, I-16145 Genova, Italy. (blx@diam.unige.it)

L. Cavallaro, E. Foti, R. E. Musumeci, and P. Scandura, Department of Civil and Environmental Engineering, University of Catania, Viale A. Doria 6, I-95125 Catania, Italy. (lcavalla@dica.unict.it; efoti@dica.unict.it; rmusume@dica.unict.it; pscandu@dica.unict.it)